In-Flight Detection of Vibration Anomalies in Unmanned Aerial Vehicles

Portia Banerjee *
Research Engineer, Member of ASME
Diagnostics and Prognostics Group
SGT Inc., NASA Ames Research Center
Moffett Field, CA 94035.
Email: portia.banerjee@nasa.gov

Wendy A. Okolo
Aerospace Research Engineer
Diagnostics and Prognostics Group,
NASA Ames Research Center
Moffett Field, CA 94035.
Email: wendy.a.okolo@nasa.gov

Andrew J. Moore
Aerospace Research Engineer
Dynamic Systems and Control Branch
NASA Langley Research Center,
1 Nasa Dr, Hampton, VA 23666
Email: andrew.j.moore@nasa.gov

Owing to the frequency of occurrence and high risk associated with bearings, identification and characterization of bearing faults in motors via nondestructive evaluation (NDE) methods have been studied extensively, amongst which vibration analysis has been found to be a promising technique for early diagnosis of anomalies. However, a majority of the existing techniques rely on vibration sensors attached onto or in close proximity to the motor in order to collect signals with a relatively high SNR. Due to weight and space restrictions, these techniques cannot be used in unmanned aerial vehicles (UAVs), especially during flight operations since accelerometers cannot be attached onto motors in small UAVs. Small UAVs are often subjected to vibrational disturbances caused by multiple factors such as weather turbulence, propeller imbalance or bearing faults. Such anomalies may not only pose risks to UAV's internal circuitry, components or payload, they may also generate undesirable noise level particularly for UAVs expected to fly in low-altitudes or urban canyon. This paper presents a detailed discussion of challenges in in-flight detection of bearing failure in UAVs using existing approaches and offers potential solutions to detect overall vibration anomalies in small UAV operations based on IMU data.

1 Introduction

The integration of small unmanned aerial vehicles (UAVs) for parcel delivery, surveillance, weather monitoring, precision agriculture and other applications will have an effect on the national airspace in the coming years [1, 2]. Thus, it is imperative to identify and prepare for potential hazards or risks associated with these vehicles. Hazards relevant to small UAVs may include flight deviation outside approved airspace, proximity to static and dynamic obstacles, loss of control and critical system failure such as loss of navigation or communication link and degraded power-train system or mechanical faults. A systematic approach is thus required for in-flight non-destructive evaluation (NDE) and health monitoring of UAVs in order to enable efficient and safe operations in the low-altitude airspace as well as mitigate associated risks to people and property on ground [3]. With that objective, NASA's Aeronautics Research Mission Directorate describes a strategic plan for investigating and advancing in-time safety assurance capabilities [4] by integrating information from multiple sources. Information may be (1) vehicle specific such as battery state-of-charge, component's health status, (2) from third-party sources such as weather, obstacles and terrain information providers or (3) from UAV Traffic Management (UTM) such as real-time traffic within an airspace.

Among critical power-plant components in UAVs are motors that include rolling parts called bearings and propellers. Similar to other mechanical systems, bearings in UAVs are prone to fatigue degradation over time leading to motor failure, which in turn may interfere with nominal operations of the hub, spinner and propeller. In order to study risk associated with bearing failures in UAV motors, a report released by the Department of Aerospace Engineering and Mechanics at the University of Minnesota on failure mode and effect analysis (FMEA) in a small low-cost unmanned UAV, was reviewed [5]. The experimental flight test hardware consisted of a fixed-winged electric aircraft, as shown in Fig 1, provided by the NASA Langley Research Center with a wide

*Corresponding author.

array of sensors for data collection along with a 6 degrees-of-freedom aerodynamic simulation model at the core of its flight research platform. A summary of motor FMEA , as reported in [5], is presented in Table 1. The cause for each failure mode in the motor has been identified and their effects are classified in terms of likelihood and criticality. Although likelihood of bearing failures is medium (M), they are associated with high criticality of 1, which represents a fatal failure mode that could result in damage to the vehicle or property, serious injury or even loss of life, according to the Flight Assurance Procedure released by NASA Goddard Space Flight Center [6]. Hence, it is imperative to develop in-time and reliable bearing failure diagnostic and monitoring capability for enabling safe UAV operations in the future.

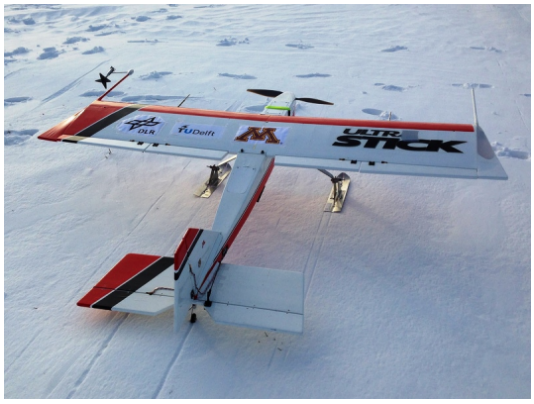

Fig. 1. Ultra Stick 120 'Ibis' UAV for FMEA study at University of Minnesota [5].

Current practice for ensuring safety of the motors includes a prescribed pre-flight and post-flight inspection of the motors followed by replacement of the bearing parts if a motor is 'felt' to be warmer or noisier than its counterparts [7]. Although bearings, like any component undergoing fatigue, are not supposed to fail instantaneously during a short flight of 1-2 hours, lack of in-flight monitoring and highly subjective nature of the prescribed checks occasionally lead to unprecedented motor failures [5]. Besides intrinsic fatigue failure causes or environmental elements such as moisture or grains of sand may get caught in between the rotor and stator inside a motor, thereby affecting its motion and aggravate a previously undetected fault. Current practice assumes periodic replacement of parts in lieu of condition-based-maintenance. However this assumption relies on a potentially costly maintenance regime that is not always adhered to.

Previous studies have demonstrated vibration analysis as a successful NDE technique to detect faults in rolling bearings. Prior research [8, 9] validates bearing fault detection methods on experimental vibration data recorded in ideal conditions wherein accelerometers are attached on to the motor frame. The output vibration signal from those testbeds contains strong signatures from bearing faults which can be diagnosed with relatively high confidence. On the other hand, in most commercial small UAVs, especially in the rotor-type vehicles, accelerometers cannot be attached onto each motor due to weight and space constraints. This is the main reason behind the gap in existing research and practical implementation of bearing fault diagnostics in small UAVs. Most UAVs are equipped with a single Inertial Measurement Unit (IMU) which consists of a tri-axial accelerometer attached onto the main frame of the vehicle. A fault signal from the IMU is often buried within noise from other sources such as external turbulences and propeller imbalances. However, such IMU data can be used to identify vibrational disturbances experienced by the UAV which may arise from a faulty motor. It is imperative to detect vibrational anomalies during a UAV flight owing to the risk posed on UAV circuitry or payload when exposed to abnormal vibrations. Techniques such as wavelet transforms [8, 10, 11] and artificial neural network (ANN) [12] have been employed to enhance diagnostic features for early detection of faults. Such techniques, although highly effective, require high computational resources. Caciotta et al. [13] have described an envelope analysis technique tested on simulations of signals from a triaxial accelerometer mounted on a electric motor in UAV. However, that study did not evaluate their bearing diagnostic techniques on real UAV flight data.

This paper presents an overview of existing studies on bearing fault detection on laboratory datasets. Accelerometer signals recorded by a IMU mounted on a real octocopter flight with faulty bearings are depicted and compared with laboratory data. Vibrational signatures from IMU acceleration data are extracted based on their frequency spectral representation, and a in-flight vibration anomaly detection approach based on tracking non-unique frequency components is demonstrated.

2 Bearing Fault Detection in Laboratory Datasets

In order to study and implement existing methods for bearing fault diagnostics, public datasets from laboratory experiments are analyzed in this section. Run-to-failure tests were performed on bearings by the Center for Intelligent Maintenance Systems (IMS) at the University of Cincinnati, under normal load conditions and the data is available in the NASA Ames Prognostic Center of Excellence dataset repository [14]. The test rig consisted of four bearings on one shaft driven by an AC motor. Accelerometers were attached onto each bearing using adhesives, as depicted in Fig. 2, to record continuous vibration signals over the entire life-span of each bearing.

The vibration data for all four bearings along with additional details of the test set up is available in [8]. Vibration data from the accelerometers was collected every 20 minutes at a sampling rate of 20 kHz by a National Instruments $DAQCard-6062E$ data acquisition device. Damage to the rolling ball in bearing 4 took 35 days to mature from a healthy state to complete failure. Since bearings are rolling components, it is evident that any damage in the bearing shows up as a periodic pattern in the vibration signal which can be extracted from its frequency spectrum. Vibration sig-

	Failure Mode	Cause	Likelihood	Effects	Criticality	Risk	Controls
Motor: Turns hub, spinner, and propeller to generate thrust							
a	Bearing failure	• insufficient lubrication	M	• motor spins with difficulty or not at all • loss of thrust LOM, LOC, LOV	1	H	• scheduled maintenance • pre-/post-flight inspection
b	Short circuit at coil	• unbalanced propeller vibration	L	• stuck motor • loss of thrust • LOM, LOC, LOV	1	M	• scheduled maintenance • pre-/post-flight inspection
c	Loose windings	• unbalanced propeller vibration	L	• incorrect motor speed • LOC, LOM	3	L	• scheduled maintenance • pre-/post-flight inspection

Table 1. FMEA of motors in Ibis UAV flight experiments at UMN [5].

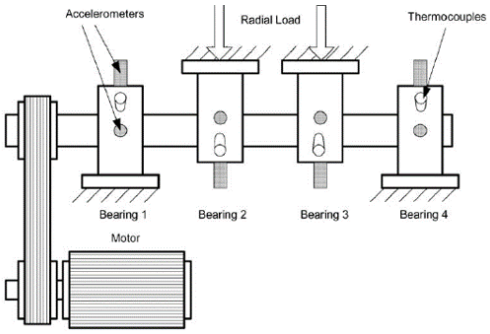

Fig. 2. Schematic of bearing test rig from IMS [14].

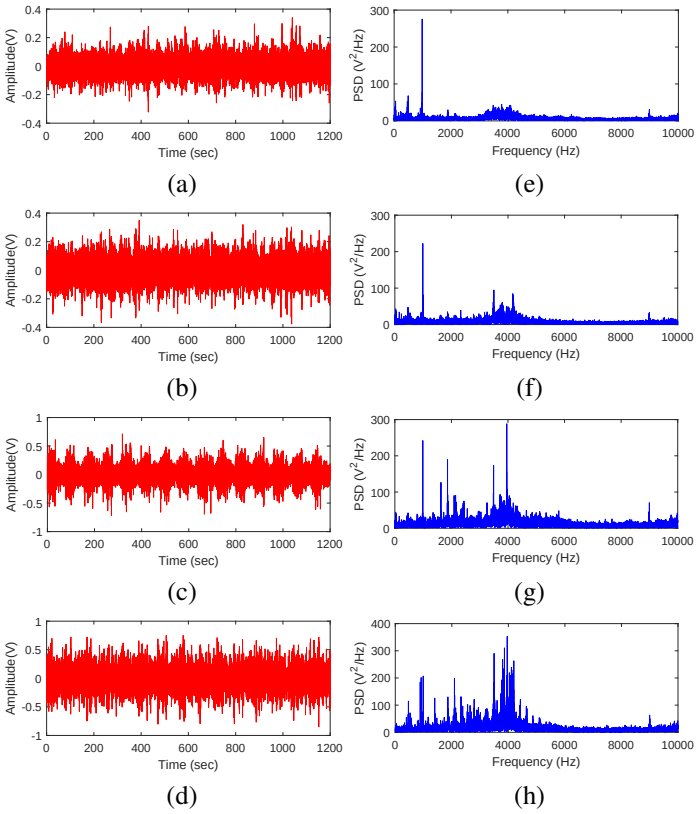

Fig. 3. Vibration signal from bearing 4 and its power spectral density at different stages of failures (a) Day 5 (b) Day 15 (c) Day 25 and (d) Day 35.

nals from the accelerometer attached to bearing 4 obtained at the 5^{th}, 15^{th}, 25^{th} and 35^{th} days are depicted in Fig. 3 (a)- (d). The corresponding power spectral density (PSD) at different frequency components, shown in Fig. 3 (e)- (h) indicates clear distinction between the bearings at the different stages of degradation.

In order to study the damage propagation over the entire 35 days, the PSD of the vibration signal was computed and then the 7 frequencies with highest PSD values were plotted in Fig. 4. It can be observed that the most damage growth signatures are captured by the 5th, 6th and 7th frequencies and not by the highest PSD frequencies since the defect information is suppressed by the natural modal components of the bearing in them. A weak degradation trend is observed for the majority of bearing life, and damage grows abruptly towards the end-of-life (EOL), as noted in previous studies [8, 12]. As a result, although peak frequencies and associated PSD values may be sufficient features to discriminate bearing health at the beginning and end of its life, classification using these features during shorter time periods within the life cycle becomes challenging.

Fig. 5 (a) represents the feature space formed by 5^{th} – 10^{th} highest PSD values and the associated frequencies at the

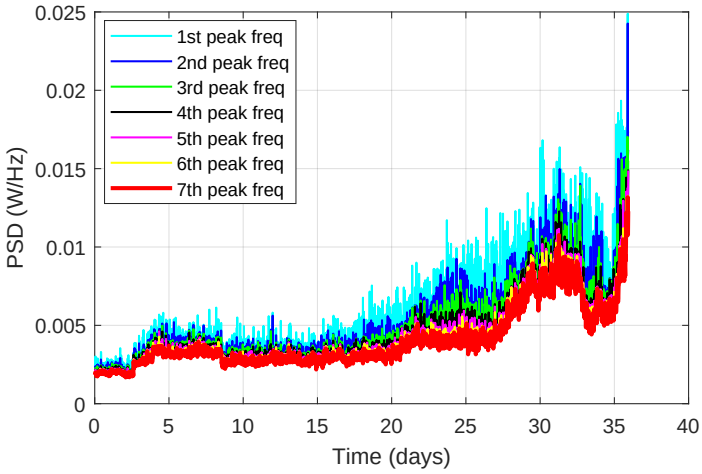

Fig. 4. Power density at first 7 peak frequency components of bearing 4 vibration data.

four different stages of the bearing life as denoted in Fig. 3. Similarly, Fig. 5 (b) represents the same feature space for signals collected at one hour intervals in the period from 6 to 3 hours before EOL of the faulty bearing. It can be observed that the features in Fig. 5 (b) highly overlap and the PSD values are not indicative of the damage growth. Thus, the ranked PSD representation of signals collected at 5 day intervals (Fig. 5 a) reveals clustering which correlates with bearing age, but is otherwise undiagnostic. Since in this paper we are interested in detecting bearing failure in UAV flights of 1-2 hour duration, PSD features of the vibration signal are deemed unsuitable for in-flight diagnosis. Hence, it is necessary to develop discriminatory features that can track any anomaly in motor bearings over a short time course which can produce a fault diagnostic within minutes.

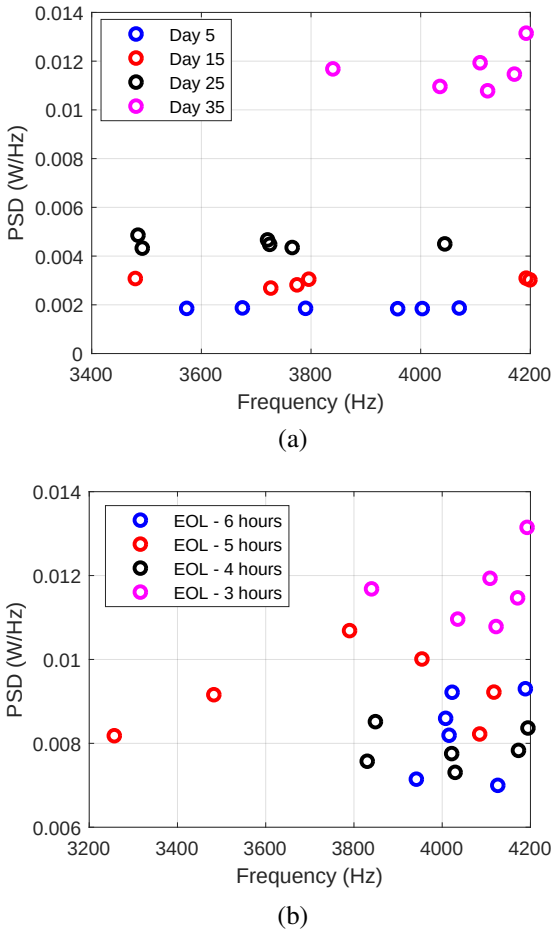

Fig. 5. Feature space for classifying bearing's state-of-health (a) For day 5, 15, 25 and 35 (b) for 6 hours, 5 hours, 4 hours and 3 hours before EOL.

3 Vibrational Anomaly Detection in Experimental UAV flights

The goal of this study is to detect vibrational anomalies in UAV motors using existing sensors from commercial UAVs without having prior information of the motor's state of health at the beginning of the flight. This section describes the acceleration data obtained from experimental UAV flights and the challenges of implementing existing methods on such data. Further, the proposed approach of generating an vibrational anomaly indicator based on non-unique frequency tracking is presented.

3.1 Experimental flight set-up

UAV flight experiments were performed at the NASA Langley Research Center on a *DJI S1000* octocopter, as shown in Fig. 6. The vehicle was equipped with Pixhawk autopilot hardware (`http://pixhawk.org/`) and commanded with Ardupilot software (`http://ardupilot.org/`). For some of the flight tests, the octocopter was flown with a faulty bearing on one of the UAV motors and stopped before the bearing reached total failure to avoid an incident or damage to the vehicle. Data from the Pixhawk IMU package (tri-axial accelerometer, gyroscopes and magnetometer), filtered to 25 Hz, was analyzed later in playback mode to obtain diagnostic features indicative of bearing faults. The vibration data along x-direction has been analyzed and reported in this paper. It was found that acceleration data in either x or y direction could be used to detect vibrational anomalies. However, data in z-direction had higher noise especially since IMU measurements were significantly affected during landing and take-off of the UAV, and were not representative of any vibrational anomalies. This observation aligned to previous findings reported in [15].

Flight #	Duration (sec)	Status
F1	2500	Healthy
F2	1700	Healthy
F3	2400	Faulty bearing
F4	3200	Faulty bearing
F5	1500	Unknown

Table 2. Experimental flight dataset for bearing fault detection.

Fig. 6. *DJI S1000* octocopter used for flight tests.

IMU accelerometer data from a total of five flights F_1, F_2, F_3, F_4, F_5 were studied in this experiment. Data from $F_1 - F_4$ were used to extract relevant features, develop the diagnostic methodology and train the algorithm, whereas IMU data for flight F_5 was used to test the proposed method. The duration of each flight along with the health status is reported in Table 2.

3.2 Methodology

Before presenting the proposed diagnostic framework, the evaluation of existing features as described in Section 2, is implemented on the UAV dataset. Fig. 7 depicts vibration signals along the x-direction as measured by the accelerometer for (a) a healthy UAV from F_1 and (b) a UAV with faulty bearings F_3. No significant differences can be observed in the two time series. Features similar to those used in the IMS data analysis, consisting of peak frequencies and PSD values, were extracted from the accelerometer data. For generating the feature space in Fig. 8, the entire flight of 2500 seconds was divided into 5 sections of 500 seconds each whose features are respectively denoted by red, blue, green, black and pink colors starting from beginning to end of flight. Each 500 seconds section is further segmented into 4 windows of 125 seconds each. The PSD was computed for each of these windowed signals and the $5^{th} - 10^{th}$ frequencies with highest PSD values were plotted with a set of symbols of a particular color, defined in Fig. 7. The red markers indicate features from the first 500 seconds (≈ 8 min) of the UAV flight whereas the pink markers indicate features from the last 8 minutes of the UAV flight.

No feature discrimination can be observed between healthy and faulty bearings in the PSD representation. Similar to the laboratory dataset depicted in Fig. 5 (b), a trend correlated to age is expected, for example between the early red (0-500 sec epoch) and black or pink symbols in the feature plot in the case of faulty bearings, since the PSD for faulty bearings is high relative to the PSD of a healthy state. While, some of the black and pink symbols are separated in Fig. 8 (b), many of those symbols overlap with the feature points with low PSD values. Moreover, the PSD values for the peak frequencies in the healthy bearing signal lies in the same range as those of the faulty bearing. This is due to the fact that (unlike laboratory conditions) the signal is recorded by an accelerometer within the IMU which is located at the central frame of the UAV. The signal is attenuated, due to sensor placement far from the motor with faulty bearings, vibrations from several sources including external turbulence, imbalanced propellers and possibly other component anomalies. With such signal attenuation and intermixing, it is not surprising that no useful health information could be extracted from these feature plots.

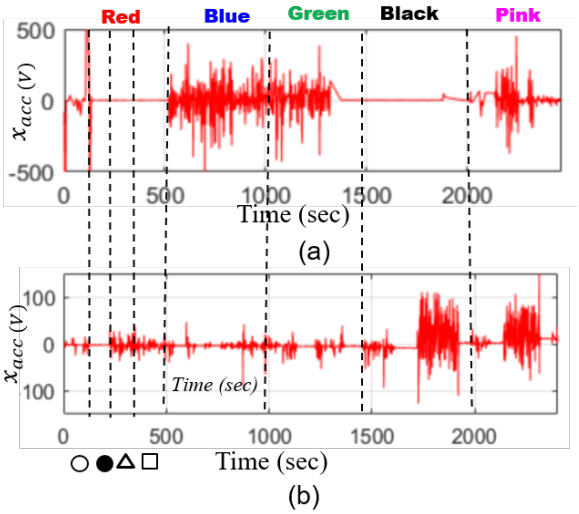

Fig. 7. Experimental flight dataset for vibrational anomaly detection.

Thus, we present a novel approach for extracting vibrational anomaly information based on tracking non-unique frequency components generated from IMU data on a UAV with faulty bearings. From Fig. 8 (a), it is seen that the features are aligned in separate unique bins unlike the feature space in Fig. 8(b). This signifies that even if PSD values of IMU data from healthy flights lied in the same range as those with faulty bearings, the frequency components matched with the natural or previously encountered frequencies recorded by the IMU during the UAV flight. No new frequency components showed up even when they exhibited high PSD values. On the other hand, in the IMU signal for a faulty bearing, newer frequency components are generated which do not match with previously observed unique frequencies. This observation can be explained by the change in modal properties of a mechanical structure in the presence of a crack [16]. Based on this observation, the features comprising peak frequencies and PSD values from the windowed signals are plotted in the feature space and then assigned in a total of N_t unique frequency bins. As more windowed signals are analyzed and their features are plotted, the number of non-unique frequency components are counted, denoted by N_f. A normalized health diagnostic feature named as Vi-

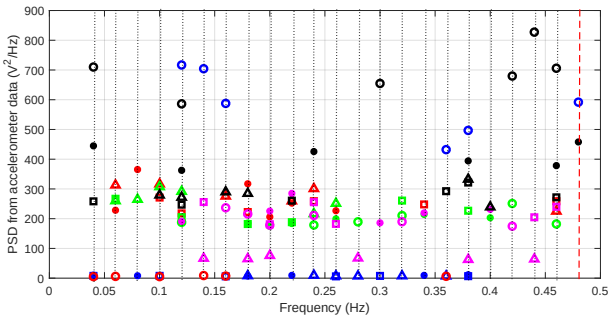

(a)

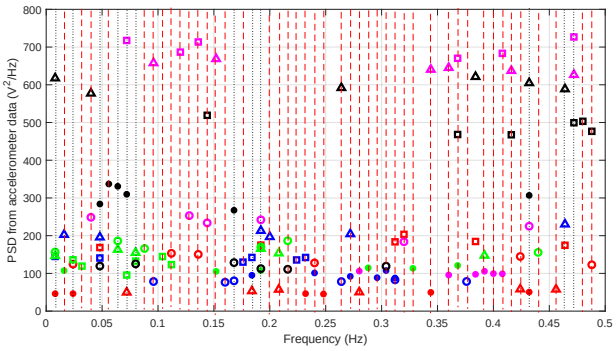

(b)

Fig. 8. Feature space from IMU data for classifying state-of-health of UAV flight with (a) Healthy bearing (b) Faulty bearing.

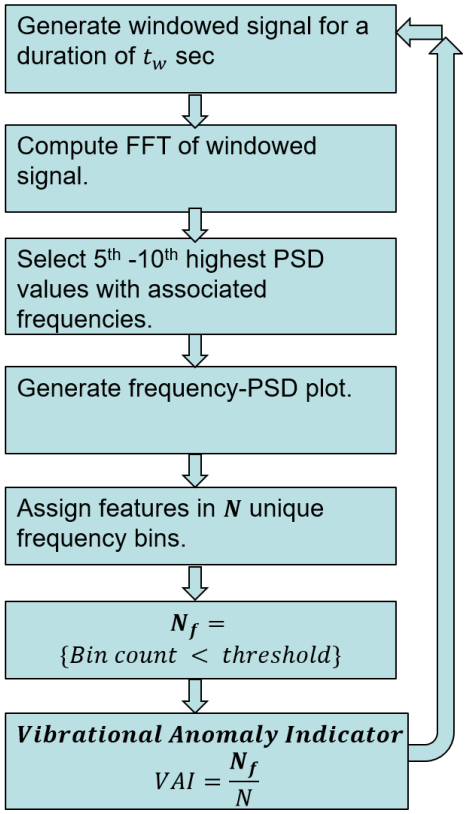

Fig. 9. Proposed algorithm for in-time tracking of vibration anomalies in UAV flights.

brational Anomaly Indicator (VAI) is then defined as:

$$VAI = \frac{N_f}{N_t} \tag{1}$$

The entire process of tracking unusual vibration status in the UAV during its flight is summarized in a flowchart in Fig. 9. In Fig. 8 (a), the bins consisting of features with unique frequencies have been marked with straight lines. IMU data from flights $F_1 - F_4$ with known health status were used to generate the 'threshold' parameter or the value of bin count less than which a frequency bin would be identified as a non-unique frequency. In this study, the parameter value was $threshold = 3$. The bins which have at least greater 3 features are assumed to represent its modal characteristics and are denoted with black dashed lines whereas the bins with fewer than 3 features are identified as the non-unique components, denoted with red dashed lines. Here, the modal frequency indicates the frequency components of signal in normal condition. As observed, the number of non-unique frequency components are higher in the case of faulty bearings and hence it is associated with a high VAI metric.

4 Results and Discussion

The proposed approach was trained using the accelerometer data from flights $F_1 - F_4$. The feature plots generated from the IMU data in the healthy flights $F_1 - F_2$ are shown in Fig. 10 (a-b) whereas those for flights with anomalous vibrations $f_3 - F_4$ are shown in Fig. 10 (c-d) . The PSD values of flight data $F_3 - F_4$ are not distinct from those of the healthy flights and hence not indicative of any faulty bearing.

However, as observed from Fig. 10 (a-b), in the absence of faults, no new frequency components appeared during the entire flight. Assuming that the flights began with healthy bearings, the frequency components generated from the first signal window represents the modal frequencies of the healthy bearings. When fault either appeared or degraded in one of the motor bearings during the flight, the peak frequencies did not align in unique frequency bins representing frequency components other than the modal frequencies, as depicted in Fig. 10 (c-d). The *VAI* computed for the four flights were as follows: (a) 0.04 for F_1 (b) 0.08 for F_2 (c) 0.65 for F_3 and (d) 0.84 for F_4.

For validation, the proposed diagnostic feature *VAI* was computed for a UAV flight with unknown bearing status. The flight F_5 was scheduled to be operating within line-of-sight and no bearing issues were identified during pre-inspection. However, after 1500 seconds from the beginning of the flight, abnormal noise was heard from one of the UAV motors which lead to its forced termination. The IMU data, shown in Fig. 11 was then analyzed in a playback mode to generate its frequency-PSD feature plot (Fig. 12(a)) and compute the associated *VAI*. As shown in Fig. 12(b) gradual increase of *VAI* can be observed starting from 0 at the beginning of flight. This confirms that the modal frequencies did

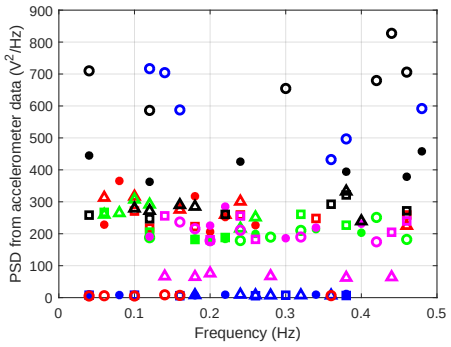

(a)

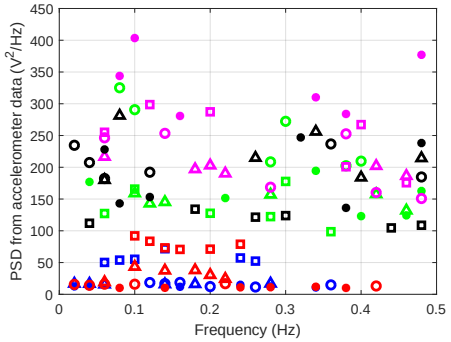

(b)

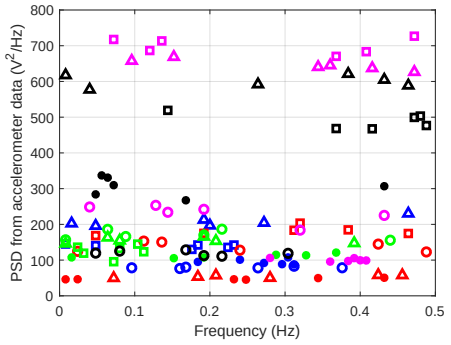

(c)

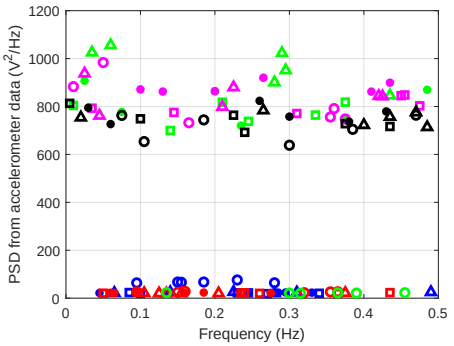

(d)

Fig. 10. Feature space from IMU data of UAV flights (a) F_1 (b) F_2 (c) F_3 and (d) F_4.

not show anomalies at the beginning of the flight. However, at around 600 seconds the *VAI* begins to increase and continues increasing till the end of the 1500-second long flight. Additional investigation revealed that F_5 was one of the flight tests conducted with the bearing fault on the motor. Hence it was verified that *VAI* can be used as a potential in-time diagnostic feature of state-of-health of the UAV exposed to vibration anomalies caused by faulty bearings. However, it should be noted that although the current results are based on acceleration data obtained from UAV flights with faulty bearings, IMU measurements restricts fault diagnosis only to vibrational anomalies which may or may not originate from a faulty bearing. Additional information, particularly acceleration data collected at higher frequencies, should be analyzed to isolate the source of such anomalous vibrations.

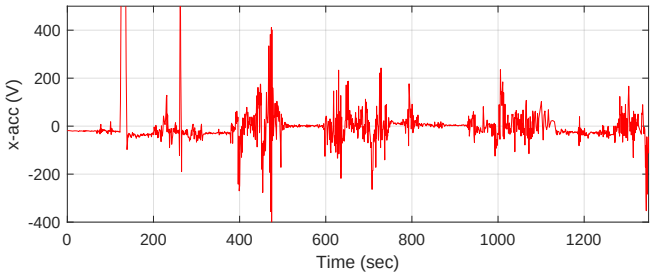

Fig. 11. IMU accelerometer signal for test flight F_5.

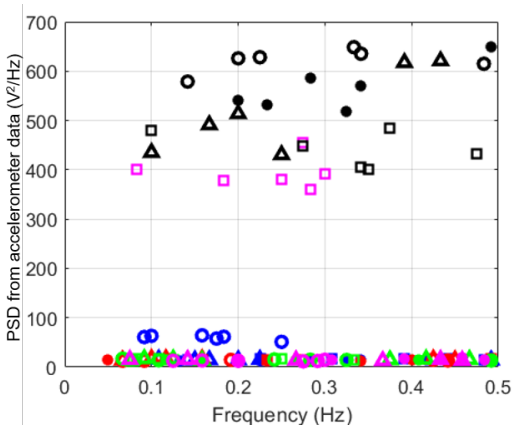

(a)

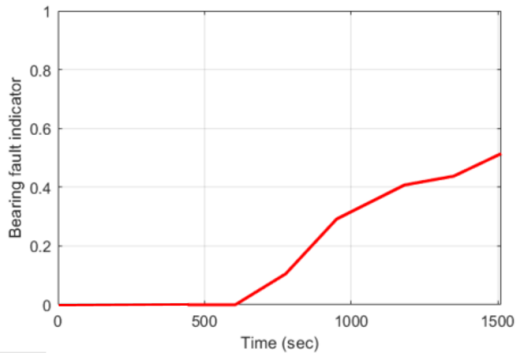

(b)

Fig. 12. (a) Feature space from IMU data in test UAV flight F_5 (b) *VAI* computed in-time from the feature plot.

5 Conclusion

In this paper, criticality of in-flight diagnostics for UAV motors was studied. Comparison of bearing fault diagnosis methods on a laboratory dataset and from flight experiments on commercial UAVs were performed. Vibration data from the IMU located at the central frame of a UAV was analyzed and utilized in the development of a vibration anomaly indicator (VAI). The VAI was defined based on counting the non-unique frequency components in the feature space of the UAV vibration data.

Although the health indicator was demonstrated on flights designed with faulty bearings, one of challenges of the proposed method is that the health indicator can detect an anomaly but not isolate the source of it. Data from central IMU contains other information inherent to the vehicle, thus other sensors such as temperature or current measurements should be used in addition to the IMU to refine the diagnostic results and identify which motor or bearing failed. Further, it is important to integrate the physics of bearing failures and degradation with the IMU measurement data in order to improve diagnostics and extend to in-flight prognostic application. Finally, the proposed approach shall be demonstrated on additional flight test data to verify its benefit and extend the development.

Acknowledgements

This work was supported by the System-Wide Safety (SWS) project under the Airspace Operations and Safety Program within the NASA Aeronautics Research Mission Directorate (ARMD). The authors thank Dr. Patrick Quach from the Safety Critical Avionics Branch at NASA Langley Research Center for the flight data utilized in this paper.

References

[1] Kopardekar, P., Rios, J., Prevot, T., Johnson, M., Jung, J., and Robinson, J. E., 2016. "Unmanned aircraft system traffic management (utm) concept of operations". In AIAA Aviation Forum, AIAA.

[2] FAA, 2018. Unmanned aerial system (uas) traffic management (utm), concept of operations. Tech. rep., Federal Aviation Administration.

[3] Corbetta, M., Banerjee, P., Okolo, W., Gorospe, G., and Luchinsky, D. G., 2019. "Real-time uav trajectory prediction for safety monitoring in low-altitude airspace". In AIAA Aviation 2019 Forum, p. 3514.

[4] NASA, 2017. "Aeronautics research mission directorate strategic implementation plan". *[Online] https://www.nasa.gov/aeroresearch/strategy*.

[5] Freeman, P. M., 2014. "Reliability assessment for low-cost unmanned aerial vehicles".

[6] NASA Goddard Space Flight Center, Greenbelt, M. U., 2009. "Flight assurance procedure p-302-720: Performing a failure modes and effects analysis".

[7] Byers, C. C., and Salgueiro, G., 2017. Pre-flight self test for unmanned aerial vehicles (uavs), Jan. 10. US Patent 9,540,121.

[8] Qiu, H., Lee, J., Lin, J., and Yu, G., 2006. "Wavelet filter-based weak signature detection method and its application on rolling element bearing prognostics". *Journal of sound and vibration,* **289**(4-5), pp. 1066–1090.

[9] Kumar, A., and Kumar, R., 2019. "Signal processing for enhancing impulsiveness towards estimating location of multiple roller defects in a taper roller bearing". *Journal of Nondestructive Evaluation, Diagnostics and Prognostics of Engineering Systems*, pp. 1–25.

[10] Yan, R., and Gao, R. X., 2008. "Rotary machine health diagnosis based on empirical mode decomposition". *Journal of Vibration and Acoustics,* **130**(2), p. 21007.

[11] Liu, J., Wang, W., and Golnaraghi, F., 2008. "An extended wavelet spectrum for bearing fault diagnostics". *IEEE Transactions on Instrumentation and Measurement,* **57**(12), pp. 2801–2812.

[12] Yu, Y., Junsheng, C., et al., 2006. "A roller bearing fault diagnosis method based on emd energy entropy and ann". *Journal of sound and vibration,* **294**(1-2), pp. 269–277.

[13] Caciotta, M., Cerqua, V., Leccese, F., Giarnetti, S., De Francesco, E., De Francesco, E., and Scaldarella, N., 2014. "A first study on prognostic system for electric engines based on envelope analysis". In 2014 IEEE Metrology for Aerospace (MetroAeroSpace), IEEE, pp. 362–366.

[14] Lee, J., Qiu, H., Yu, G., and Lin, J., 2009. "Rexnord technical services (2007).'bearing data set', ims, university of cincinnati. nasa ames prognostics data repository".

[15] Bondyra, A., Gasior, P., Gardecki, S., and Kasiński, A., 2017. "Fault diagnosis and condition monitoring of uav rotor using signal processing". In 2017 Signal Processing: Algorithms, Architectures, Arrangements, and Applications (SPA), IEEE, pp. 233–238.

[16] Banerjee, P., Chakraborty, D., and Rinker, T., 2017. "Damage detection using time-frequency decay-rate based features". In 2017 IEEE International Conference on Prognostics and Health Management (ICPHM), IEEE, pp. 143–147.